Theoretical investigation of nonhydrostatic effects on convectively forced flows: Propagating and evanescent gravity-wave modes

Jaemyeong Mango Seo (서재명), Jong-Jin Baik (백종진), and Hye-Yeong Chun (전혜영)

Citation: Physics of Fluids **30**, 126604 (2018); doi: 10.1063/1.5053444
View online: https://doi.org/10.1063/1.5053444
View Table of Contents: http://aip.scitation.org/toc/phf/30/12
Published by the American Institute of Physics

Theoretical investigation of nonhydrostatic effects on convectively forced flows: Propagating and evanescent gravity-wave modes

Jaemyeong Mango Seo (서재명),[1] Jong-Jin Baik (백종진),[1,a)]
and Hye-Yeong Chun (전혜영)[2]
[1]*School of Earth and Environmental Sciences, Seoul National University, Seoul 08826, South Korea*
[2]*Department of Atmospheric Sciences, Yonsei University, Seoul 03722, South Korea*

(Received 23 August 2018; accepted 2 December 2018; published online 28 December 2018)

Nonhydrostatic effects on convectively forced mesoscale flows are theoretically investigated using a linearized, two-dimensional, steady-state, nonrotating, Boussinesq airflow system with prescribed convective forcing. The nondimensionalized airflow system contains the nonhydrostaticity factor $\beta = U/Na$, where U is the basic-state wind speed, N is the basic-state buoyancy frequency, and a is the half-width of the convective forcing. In an inviscid-limit system, the solution for vertical velocity is classified into the propagating mode ($k \le \beta^{-1}$, where k is the nondimensional horizontal wavenumber) and the evanescent mode ($k > \beta^{-1}$). As β increases, an alternating wavy pattern of updrafts and downdrafts appears downstream of the convective forcing with a nondimensional horizontal wavelength of $2\pi\beta$ corresponding to the nondimensional critical horizontal wavenumber $k_c = \beta^{-1}$. The momentum flux analysis shows that the alternating updrafts and downdrafts are almost horizontally propagating gravity waves of the propagating mode whose k is slightly smaller than k_c and that these gravity waves strengthen the momentum flux above the convective forcing. In a viscous system, the solution for vertical velocity has propagating and decaying components simultaneously that cannot be explicitly separated. Here, the propagating mode and two evanescent modes are defined by comparing the magnitudes of the nondimensional vertical wavenumber and decay rate. For large viscous coefficients, the k-range of the propagating mode becomes narrow and the alternating updrafts and downdrafts are dissipated. As β increases, the propagating mode, which strengthens the momentum flux above the convective forcing, is effectively dissipated even with a small viscous coefficient. *Published by AIP Publishing.* https://doi.org/10.1063/1.5053444

I. INTRODUCTION

Internal waves in fluids are interesting and important phenomena and have received much attention in fluid mechanics, atmospheric sciences, oceanography, and so on.[1–5] There are many mesoscale phenomena whose basic dynamics can be understood by theoretically examining the response of a stably stratified atmosphere to specified thermal forcing such as condensational heating in convective clouds or evaporative cooling of raindrops in the boundary layer. Along this line of research, extensive studies have been performed to better understand the dynamics of thermally forced flows (see Ref. 6). The equation systems used so far are diverse, ranging from the simplest system of two dimensions and constant basic-state wind speed and buoyancy frequency[7] to complex systems of, for example, three dimensions and shear flow with a critical level.[8]

One of the troublesome factors in theoretical studies of thermally forced flows is the nonhydrostaticity of the airflow system. Hydrostatic approximation, which is valid in a system when the horizontal length scale of motion is much larger than the vertical length scale of motion, simplifies mathematical problems greatly because inertial terms in the vertical momentum equation are neglected under this approximation. However, in some deep convection problems, the vertical length scale of motion can be comparable to the horizontal length scale of motion, thus invalidating the hydrostatic approximation. In spite of this fact, very little attention has been paid to nonhydrostatic effects on convectively forced mesoscale flows.

Many studies of nonhydrostatic effects on orographically forced mesoscale flows, especially mountain waves, have been made. Queney[9] indicated that in a nonhydrostatic system with vertically uniform basic-state wind speed and static stability, lee waves with the dimensional horizontal wavelength equal to $2\pi k_c^{-1}$, where k_c is the dimensional critical horizontal wavenumber, are evident when the half-width of a bell-shaped mountain is $\sim k_c^{-1}$. Smith[10] overviewed the influence of mountains on the atmosphere. He classified the solution for the vertical velocity in wavenumber space into two modes depending on the sign of $l^2 - k^2$, where l [$l^2 = N^2/U^2 - (\partial^2 U/\partial z^2)/U$, where N is the basic-state buoyancy frequency and U is the basic-state wind speed] is the Scorer parameter that is determined by the vertical structure of the basic-state wind speed and static stability and k is the dimensional horizontal wavenumber. The solution with $k^2 < l^2$ represents vertically propagating gravity waves (propagating mode), and the solution with $k^2 > l^2$ represents vertically decaying gravity waves

a)Electronic mail: jjbaik@snu.ac.kr

(evanescent mode). Similar classification and associated resonant wave generation are also found in several experimental studies.[1,4,11]

In vertically structured atmospheres, vertically propagating gravity waves can be reflected according to the vertical structure of the Scorer parameter.[12,13] The reflected gravity waves can be trapped in the lower atmosphere, and these trapped waves can form lee waves. Keller[14] investigated nonhydrostatic effects on mountain waves in the presence of wind shear in the troposphere and a stability jump between the troposphere and stratosphere on the basis of Ref. 15. Broutman *et al.*[16,17] examined the behaviors of mountain waves in vertically structured hydrostatic and nonhydrostatic atmospheres using the ray theory. The nonhydrostatic effects on lee waves that are produced by a temperature inversion were investigated by Vosper[18] and Teixeira *et al.*[19]

A number of observational studies[20,21] have reported that convective clouds generate not only vertically propagating gravity waves but also slantwise/horizontally propagating gravity waves. In a numerical modeling study by Alexander and Holton,[22] the slantwise/horizontally propagating nonhydrostatic gravity waves are clearly identified in the spectrum of convectively forced gravity waves. To enhance our understanding of the dynamics of the slantwise/horizontally propagating gravity waves forced by convection, in-depth theoretical studies of nonhydrostatic effects on convectively forced gravity waves are required.

It is well-known that the wave energy transported by convectively forced gravity waves is one of the main energy sources that play an important role in maintaining the circulation of the stratosphere and mesosphere (see Ref. 23). Many researchers have developed the parameterizations of convectively forced gravity-wave drag for use in large-scale or climate models.[24–30] Note that the convectively forced gravity-wave drag parameterizations proposed are formulated in a Boussinesq system. Theoretical studies of nonhydrostatic effects on convectively forced gravity waves can be helpful in improving or developing a convectively forced gravity-wave drag parameterization.

Using a nondimensional numerical model, Woo *et al.*[31] studied nonhydrostatic effects on convectively forced mesoscale flows. They found that an alternating wavy pattern of updrafts and downdrafts appears downstream of the convective forcing and that the nondimensional horizontal wavelength in the alternating wavy pattern is approximately $2\pi\beta$ (β: nonhydrostaticity factor). These results are consistent with those of Queney.[9] Although Woo *et al.*[31] showed nonhydrostatic effects on convectively forced mesoscale flows, the analysis does not sufficiently elucidate the dynamics of convectively forced mesoscale flows in a nonhydrostatic system, particularly the dynamics of the alternating updrafts and downdrafts downstream of the convective forcing. This motivates the present study.

Among the three generation mechanisms for convectively forced gravity waves (thermal forcing, obstacle, and mechanical oscillator mechanisms), this study follows the thermal forcing mechanism. A brief review of the three generation mechanisms is given in the work of Song *et al.*[32] In the real world, thermal forcing from convective clouds varies spatio-temporally. Gravity waves forced by temporally varying thermal forcing can be obtained using the Green function method.[8,33] Pulse thermal forcing expressed by $\delta(t)$ generates waves propagating downstream.[7,8,33] Flows/waves forced by steady thermal forcing are obtained by integrating those forced by pulse thermal forcing with respect to time. In a hydrostatic system, flows/waves forced by thermal forcing are characterized by downstream propagating waves which are generated at $t = 0$ (moving mode) and standing vertically wavy structures near the thermal forcing (stationary mode).[34] In a nonhydrostatic system, a horizontally wavy structure appears between the moving mode and stationary mode. This study attempts to clarify the characteristics of the horizontally wavy structure. In this study, we consider a steady-state system with steady convective forcing to examine the system in which the horizontally wavy structure clearly appears.

The main purpose of this study is to theoretically analyze nonhydrostatic effects on convectively forced flows, particularly focusing on the analysis of propagating and evanescent modes. In Sec. II, the governing equations and solutions are presented. In Secs. III A and III B, nonhydrostatic effects in inviscid-limit and viscous systems are, respectively, presented and discussed. In Sec. III C, nonhydrostatic effects on the gravity-wave momentum flux are presented and discussed. A summary and conclusions are given in Sec. IV.

II. GOVERNING EQUATIONS AND SOLUTIONS

In this study, a two-dimensional, steady-state, nonrotating, Boussinesq airflow system with convective forcing is considered. The equations governing small-amplitude perturbations are expressed as follows:

$$U\frac{\partial u}{\partial x} = -\frac{\partial \pi}{\partial x} - \nu_m u, \tag{1}$$

$$U\frac{\partial w}{\partial x} = -\frac{\partial \pi}{\partial z} + b - \nu_m w, \tag{2}$$

$$U\frac{\partial b}{\partial x} + N^2 w = \frac{g}{c_p T_0} q - \nu_T b, \tag{3}$$

$$\frac{\partial u}{\partial x} + \frac{\partial w}{\partial z} = 0, \tag{4}$$

where u is the perturbation velocity in the x-direction, w is the perturbation velocity in the z-direction, π is the perturbation kinematic pressure, b is the perturbation buoyancy, ν_m is the coefficient of Rayleigh friction, ν_T is the coefficient of Newtonian cooling, g is the gravitational acceleration, c_p is the specific heat of air at constant pressure, T_0 is the reference temperature, and q is the convective forcing function. The basic-state wind speed in the x-direction U is constant with height in this study. Note that our system of equations represents not only a stationary convective forcing (convective system) but also a moving convective system in the basic-state wind speed $U + C$, where C is the horizontal moving speed of the convective system.

The Rayleigh friction and Newtonian cooling terms represent friction and radiative cooling, respectively, but not diffusion and thermal dissipation processes. In this study, the simplest forms of friction and radiative cooling are considered so that we can obtain analytical solutions to the equations that

include the Rayleigh friction and Newtonian cooling terms and thus examine viscous effects.

To solve the above equation system, the Green function method is used.[8,33] First, we obtain the solution for the perturbation vertical velocity in the equation system with line-type convective forcing that is given by

$$q(x,z) = q_0 \frac{a^2}{x^2+a^2}\delta(z-h), \tag{5}$$

where q_0 and a are the strength and half-width of the bell-shaped convective forcing, respectively, δ is the Dirac delta function, and h is the height at which the line-type convective forcing is located. Then, we obtain the solution for the finite-depth convective forcing by integrating the solution for the perturbation vertical velocity induced by the line-type convective forcing with respect to h.

The following dimensionless variables (with tildes) are introduced:[31,35]

$$\begin{gathered} x = a\tilde{x}, a = a\tilde{a}, \quad z = \frac{U}{N}\tilde{z}, \quad h = \frac{U}{N}\tilde{h}, \quad U = U\tilde{U}, \quad q = q_0\tilde{q}, \\ \nu_m = \frac{U}{a}\tilde{\nu}_m, \quad \nu_T = \frac{U}{a}\tilde{\nu}_T, \quad u = \frac{gq_0a}{c_pT_0NU}\tilde{u}, \quad w = \frac{gq_0}{c_pT_0N^2}\tilde{w}, \\ \pi = \frac{gq_0a}{c_pT_0N}\tilde{\pi}, \quad b = \frac{gq_0a}{c_pT_0U}\tilde{b}. \end{gathered} \tag{6}$$

After applying the above dimensionless variables to Eqs. (1)–(5), we obtain nondimensionalized governing equations and line-type convective forcing as follows:

$$\frac{\partial\tilde{u}}{\partial\tilde{x}} = -\frac{\partial\tilde{\pi}}{\partial\tilde{x}} - \tilde{\nu}_m\tilde{u}, \tag{7}$$

$$\beta^2\frac{\partial\tilde{w}}{\partial\tilde{x}} = -\frac{\partial\tilde{\pi}}{\partial\tilde{z}} + \tilde{b} - \beta^2\tilde{\nu}_m\tilde{w}, \tag{8}$$

$$\frac{\partial\tilde{b}}{\partial\tilde{x}} + \tilde{w} = \tilde{q} - \tilde{\nu}_T\tilde{b}, \tag{9}$$

$$\frac{\partial\tilde{u}}{\partial\tilde{x}} + \frac{\partial\tilde{w}}{\partial\tilde{z}} = 0, \tag{10}$$

$$\tilde{q}(\tilde{x},\tilde{z}) = \frac{\tilde{a}^2}{\tilde{x}^2+\tilde{a}^2}\delta(\tilde{z}-\tilde{h}), \tag{11}$$

where $\beta = U/Na$ is the nonhydrostaticity factor. Here, the half-width of the bell-shaped convective forcing a represents the horizontal length scale of the convective forcing. Note that the arbitrarily chosen horizontal length scale L is used in the work of Woo *et al.*[31] The nonhydrostaticity factor represents the degree of the contribution of the inertial term in the vertical momentum equation [Eq. (8)]. Note that the nonhydrostaticity factor β is equivalent to the horizontal Froude number based on the half-width of the bell-shaped orographic/convective forcing.[36,37] Hereafter, tildes are dropped for simplicity.

Equations (7)–(10) can be combined into a single equation for the perturbation vertical velocity

$$\left(\frac{\partial}{\partial x}+\nu_m\right)\left(\frac{\partial}{\partial x}+\nu_T\right)\left(\frac{\partial^2 w}{\partial z^2}+\beta^2\frac{\partial^2 w}{\partial x^2}\right)+\frac{\partial^2 w}{\partial x^2} = \frac{\partial^2 q}{\partial x^2}. \tag{12}$$

By taking the Fourier transform ($x \to k$) to Eq. (12), the differential equation for w in wavenumber space is obtained

$$\frac{\partial^2\hat{w}}{\partial z^2} + m^2\hat{w} = m_0^2\hat{q}, \tag{13a}$$

where

$$m^2 = -k^2\left\{\frac{1}{(ik+\nu_m)(ik+\nu_T)} + \beta^2\right\}, \tag{13b}$$

$$m_0^2 = -\frac{k^2}{(ik+\nu_m)(ik+\nu_T)}, \tag{13c}$$

$$\hat{q} = ae^{-ak}\delta(z-h). \tag{13d}$$

The general solution of Eq. (13a) is

$$\hat{w}_{\mathrm{L}} = A_1e^{imz} + B_1e^{-imz} \quad \text{for } 0 \le z \le h, \tag{14a}$$

$$\hat{w}_{\mathrm{U}} = A_2e^{imz} + B_2e^{-imz} \quad \text{for } z > h. \tag{14b}$$

The coefficients A_1, A_2, B_1, and B_2 can be determined by applying the flat bottom boundary condition ($\hat{w}_{\mathrm{L}} = 0$ at $z = 0$), the upper radiation condition ($B_2 = 0$ with $U > 0$), and the interfacial boundary conditions at $z = h$ that are given by

$$\hat{w}_{\mathrm{L}} = \hat{w}_{\mathrm{U}}, \tag{15a}$$

$$\frac{\partial\hat{w}_{\mathrm{U}}}{\partial z} - \frac{\partial\hat{w}_{\mathrm{L}}}{\partial z} = am_0^2e^{-ak}. \tag{15b}$$

Then, the solution for the perturbation vertical velocity induced by the line-type convective forcing in wavenumber space is obtained

$$\hat{w}_{\mathrm{L}} = i\frac{am_0^2}{2m}\left\{e^{im(z+h)} - e^{-im(z-h)}\right\}e^{-ak} \quad \text{for } 0 \le z \le h, \tag{16a}$$

$$\hat{w}_{\mathrm{U}} = i\frac{am_0^2}{2m}\left\{e^{im(z+h)} - e^{im(z-h)}\right\}e^{-ak} \quad \text{for } z > h. \tag{16b}$$

To get the solution induced by the finite-depth convective forcing, we integrate Eq. (16) from the bottom height of the finite-depth convective forcing h_1 to its top height h_2 with respect to h as follows:

$$\hat{w}_1 = \int_{h_1}^{h_2}\hat{w}_{\mathrm{L}}dh \quad \text{for } 0 \le z \le h_1, \tag{17a}$$

$$\hat{w}_2 = \int_{h_1}^{z}\hat{w}_{\mathrm{U}}dh + \int_{z}^{h_2}\hat{w}_{\mathrm{L}}dh \quad \text{for } h_1 < z \le h_2, \tag{17b}$$

$$\hat{w}_3 = \int_{h_1}^{h_2}\hat{w}_{\mathrm{U}}dh \quad \text{for } z > h_2. \tag{17c}$$

After manipulation, we can obtain the following solution in wavenumber space:

$$\hat{w}_1 = (\hat{\Omega}^+_{+2} - \hat{\Omega}^+_{+1}) - (\hat{\Omega}^-_{-2} - \hat{\Omega}^-_{-1}) \quad \text{for } 0 \le z \le h_1, \tag{18a}$$

$$\hat{w}_2 = (\hat{\Omega}^+_{+2} - \hat{\Omega}^+_{+1}) - (\hat{\Omega}^-_{-2} - \hat{\Omega}^+_{-1}) \quad \text{for } h_1 < z \le h_2, \tag{18b}$$

$$\hat{w}_3 = (\hat{\Omega}^+_{+2} - \hat{\Omega}^+_{+1}) + (\hat{\Omega}^+_{-2} - \hat{\Omega}^+_{-1}) \quad \text{for } z > h_2, \tag{18c}$$

where

$$\hat{\Omega}^{\pm'}_{\pm n} = \frac{am_0^2}{2m^2}\left\{e^{\pm' im(z\pm h_n)} - 1\right\}e^{-ak}. \tag{18d}$$

In Eq. (18d), $n = 1, 2$. Each of $\hat{\Omega}^{\pm'}_{\pm n}$ represents the wave component induced by the convective forcing. The superscript of $\hat{\Omega}$ denotes the direction of wave energy propagation, with the positive (negative) sign denoting upward (downward) wave energy propagation. In the subscript of $\hat{\Omega}$, the positive (negative) sign denotes waves reflected at the surface (non-reflected waves) and n denotes the waves originated from $z = h_n$.

Finally, the solution in physical space is obtained by numerically integrating the real part as follows:

$$w_j = \int_0^\infty \mathrm{Re}\left\{\hat{w}_j e^{ikx}\right\} dk = \int_0^\infty w_{jk}\, dk. \tag{19}$$

In Eq. (19), $j = 1, 2, 3$. The Euler forward scheme is used for the numerical integration. The convective forcing is located from $z = h_1 = 1$ to $z = h_2 = 9$. The half-width of the bell-shaped convective forcing is $a = 1$. Hereafter, for simplicity, the perturbation horizontal velocity and the perturbation vertical velocity are called the horizontal velocity and the vertical velocity, respectively.

III. RESULTS AND DISCUSSION

A. Inviscid-limit system

In an inviscid-limit system, i.e., both ν_m and ν_T are sufficiently small, individual wave components [Eq. (18d)] are approximated as

$$\hat{\Omega}_{\pm n}^{\pm'} \simeq \frac{a}{2m^2}\left\{e^{\pm' im(z\pm h_n)} - 1\right\} e^{-ak}. \tag{20}$$

In Eq. (20), the vertical wavenumber $m = (1 - \beta^2 k^2)^{1/2}$ is real if $k \le \beta^{-1}$ and purely imaginary if $k > \beta^{-1}$. The wave component in the range of $k \le \beta^{-1}$, which is sinusoidal with the vertical wavenumber m and propagates vertically, is called the propagating mode. The wave component in the range of $k > \beta^{-1}$, which exponentially decreases with a decay rate of $m' = (\beta^2 k^2 - 1)^{1/2} = -im$, is called the evanescent mode. This classification of wave components has been used in mountain-wave studies.[9,10] Note that the k-boundary of both modes $k_c = \beta^{-1}$ is the critical horizontal wavenumber introduced by Queney.[9]

The spectral vertical velocity w_{jk} in Eq. (19) is obtained by applying Eq. (20) to Eq. (18) and choosing the real part of $\hat{w}_j e^{ikx}$. The spectral vertical velocity of the propagating mode ($k \le \beta^{-1}$) is given by

$$w_{1k} = -\frac{a}{m^2} e^{-ak} \sin mz \{\sin(kx + mh_2) - \sin(kx + mh_1)\} \quad \text{for } 0 \le z \le h_1, \tag{21a}$$

$$w_{2k} = -\frac{a}{m^2} e^{-ak} \{\sin mz \sin(kx + mh_2) + \cos mh_1 \cos(kx + mz) - \cos kx\} \quad \text{for } h_1 < z \le h_2, \tag{21b}$$

$$w_{3k} = \frac{a}{m^2} e^{-ak} (\cos mh_2 - \cos mh_1) \cos(kx + mz) \quad \text{for } z > h_2, \tag{21c}$$

whereas the spectral vertical velocity of the evanescent mode ($k > \beta^{-1}$) is given by

$$w'_{1k} = -\frac{a}{m'^2} e^{-ak} \sinh m'z \left(e^{-m'h_2} - e^{-m'h_1}\right) \times \cos kx \quad \text{for } 0 \le z \le h_1, \tag{22a}$$

$$w'_{2k} = \frac{a}{m'^2} e^{-ak} \left(e^{-m'h_2} \sinh m'z + e^{-m'z} \cosh m'h_1 - 1\right) \times \cos kx \quad \text{for } h_1 < z \le h_2, \tag{22b}$$

$$w'_{3k} = -\frac{a}{m'^2} e^{-ak} e^{-m'z} (\cosh m'h_2 - \cosh m'h_1) \times \cos kx \quad \text{for } z > h_2. \tag{22c}$$

Figure 1 shows the vertical velocity fields in the cases of the nonhydrostaticity factor $\beta = 0.1$, 0.3, 0.5, and 1 in the inviscid-limit system. For $\beta = 0.1$, the flow is close to the hydrostatic flow [Fig. 1(a)]. As β increases, the flow

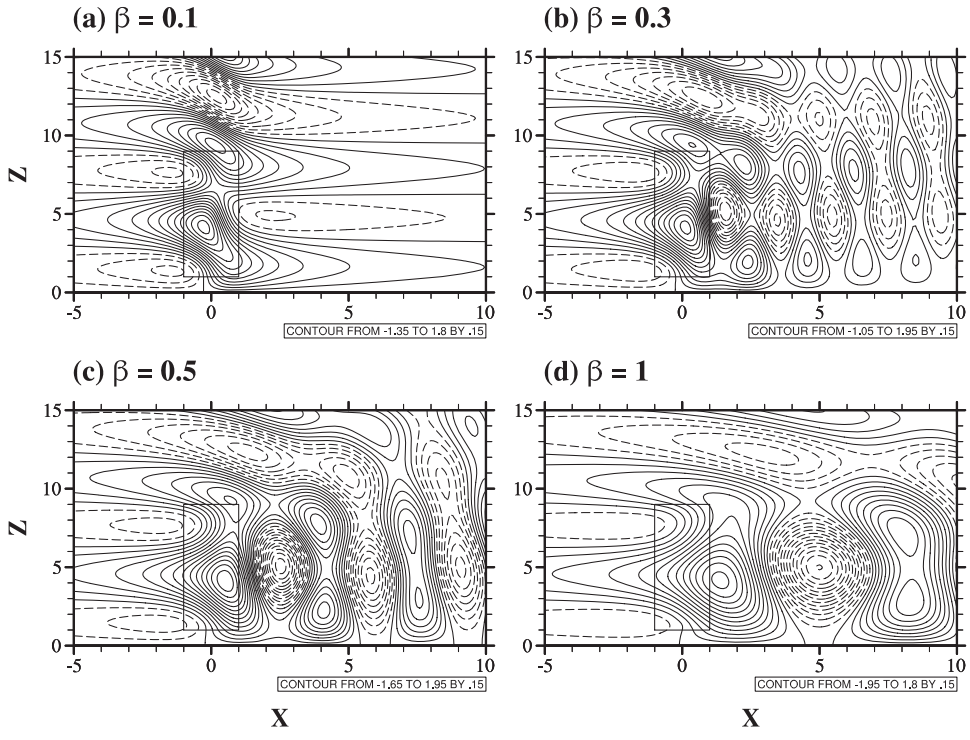

FIG. 1. Vertical velocity fields in the cases of β = (a) 0.1, (b) 0.3, (c) 0.5, and (d) 1 in the inviscid-limit system. The rectangle in each panel represents the concentrated convective forcing region. The contour line information is given at the bottom of each panel.

gradually deviates from the hydrostatic flow and becomes more non-hydrostatic. For β = 0.3, 0.5, and 1, an alternating wavy pattern of updrafts and downdrafts appears downstream of the convective forcing [Figs. 1(b)–1(d)]. The (nondimensional) horizontal wavelength ($2\pi k^{-1}$) of the alternating updrafts and downdrafts is $2\pi\beta$, which is 1.88, 3.14, and 6.28 for β = 0.3, 0.5, and 1, respectively, where $k = k_c$. Note that the dimensional horizontal wavelength of the alternating updrafts and downdrafts is $2\pi U/N$, which is fixed for uniform basic-state wind speed and static stability. The nonhydrostaticity factor β can be controlled by changing the half-width of the bell-shaped convective forcing a for given environmental conditions (fixed U and N). It can be easily seen that the alternating updrafts and downdrafts downstream of the convective forcing with the horizontal wavelength $2\pi U/N$ are generated as a decreases (β increases) in a dimensional frame.

In this study, we consider the nonhydrostatic system, so in the vertical momentum equation [Eqs. (2) and (8)], the term representing the buoyancy perturbation generated by convective forcing is balanced with the vertical pressure gradient term, the horizontal advection term, and viscous term. In the nondimensionalized vertical momentum equation [Eq. (8)], the importance of the horizontal advection term becomes apparent for large β. Like the vertically propagating wave oscillating with the frequency N, the vertical momentum perturbation experiences a vertical oscillation with the frequency N during the horizontal advection by the basic-state wind. For this reason, the dimensional horizontal wavelength of the alternating updrafts and downdrafts is U times $2\pi/N$, that is, $2\pi U/N$.

The alternating updrafts and downdrafts are almost horizontally propagating resonant waves. As the horizontal wavenumber k approaches k_c, the vertical wavenumber m of the propagating mode and the decay rate m' of the evanescent mode in the denominator of the wave components approach zero, thus amplifying corresponding wave components [see Eqs. (21) and (22)].

Note that the alternating wavy pattern is tilted upstream above the convective forcing top. In a study of flow over a mesoscale mountain in a nonhydrostatic system, Laprise and Peltier[38] showed that the generated waves propagate toward the upper-right corner of the mountain. This feature is also observed above the forcing level when the line-type convective forcing is considered (not shown).

In their numerical modeling study, Woo *et al.*[31] also found that the alternating updraft and downdraft cells appear downstream of the convective forcing and that the horizontal length scale of each cell is $\pi\beta$. Woo *et al.*[31] speculated that the alternating updraft and downdraft cells are produced by the superposition of the horizontally propagating waves of the propagating mode and the horizontally wavy pattern of the evanescent mode. We calculate the propagating mode and evanescent mode of the vertical velocity field in the case of β = 0.5 (Fig. 2). As speculated in the work of Woo *et al.*,[31] the evanescent mode exhibits a horizontally wavy pattern [Fig. 2(b)]. However, the vertical wavy pattern upstream of the convective forcing seems to be independent of β (Fig. 1). Note that the flow of the evanescent mode is much weaker than that of the propagating mode. Differences in vertical velocity field between β = 0.5 and β = 0.01 (hydrostatic-limit system) [Fig. 2(c)] and between β = 1 and β = 0.01 [Fig. 2(d)] also show that the vertically wavy pattern upstream of the convective forcing seems to be the β-independent hydrostatic-limit flow. Thus, it is deduced that the wavy pattern of the evanescent mode with small magnitude plays a role in flattening the horizontally undulating pattern of the β-independent hydrostatic-limit flow. In this study, the alternating updrafts and downdrafts

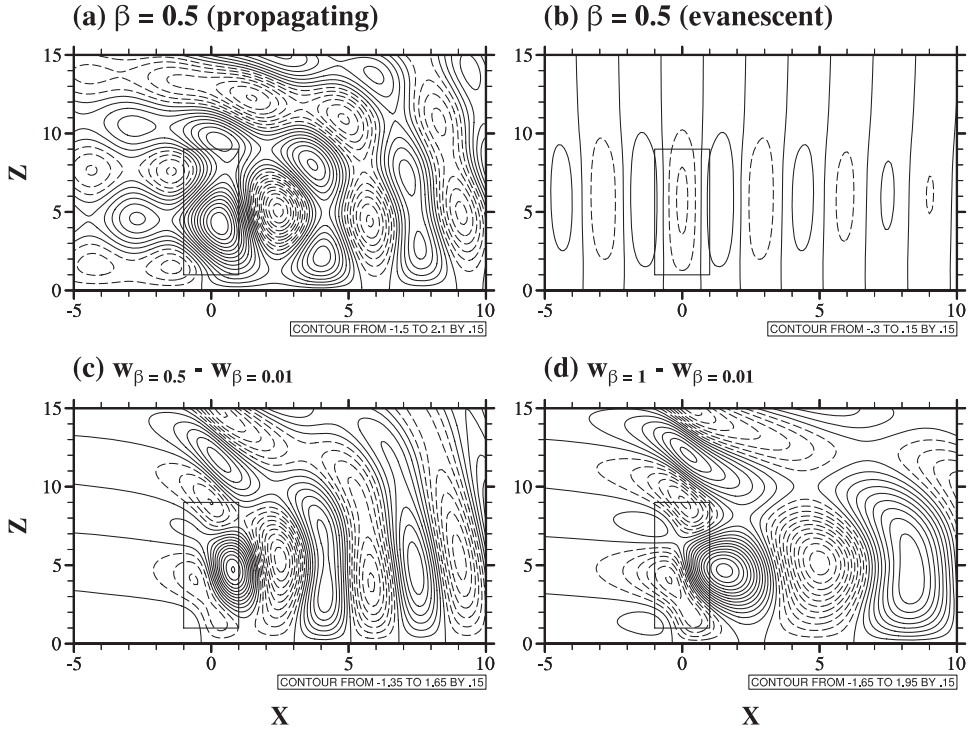

FIG. 2. Vertical velocity fields in the case of β = 0.5: (a) propagating mode and (b) evanescent mode. Differences in the vertical velocity field between the cases of (c) β = 0.5 and β = 0.01 and (d) β = 1 and β = 0.01. The rectangle in each panel represents the concentrated convective forcing region. The contour line information is given at the bottom of each panel. The inviscid-limit system is considered.

downstream of the convective forcing are regarded as the propagating mode. Note that the terminology hydrostatic-limit system used in this study means a system with sufficiently small β.

B. Viscous system

In a viscous system that includes the Rayleigh friction and Newtonian cooling, the real part of the individual spectral wave components [Eqs. (18d) and (19)] are expressed as

$$\Omega^{\pm'}_{\pm nk} = \frac{a}{2}\Big[X_R\Big\{e^{\mp' M_I(z\pm h_n)}\cos\big(kx \pm' M_R(z\pm h_n)\big) - \cos\, kx\Big\} - X_I\Big\{e^{\mp' M_I(z\pm h_n)}\sin\big(kx \pm' M_R(z\pm h_n)\big) - \sin\, kx\Big\}\Big], \tag{23a}$$

where

$$X_R + iX_I \equiv \frac{m_0^2}{m^2} = \frac{\big\{1-\beta^2(k^2-\nu_m\nu_T)\big\} - i\big\{\beta^2 k(\nu_m+\nu_T)\big\}}{\big\{1-\beta^2(k^2-\nu_m\nu_T)\big\}^2 + \big\{\beta^2 k(\nu_m+\nu_T)\big\}^2}, \tag{23b}$$

$$m = M_R + iM_I = \begin{cases} \dfrac{k(R^2+I^2)^{1/4}}{\sqrt{(k^2+\nu_m^2)(k^2+\nu_T^2)}}\left[\cos\left(\frac{1}{2}\tan^{-1}\frac{I}{R}\right) + i\,\sin\left(\frac{1}{2}\tan^{-1}\frac{I}{R}\right)\right] & \text{for } R \ge 0, \\ \dfrac{k(R^2+I^2)^{1/4}}{\sqrt{(k^2+\nu_m^2)(k^2+\nu_T^2)}}\left[-\sin\left(\frac{1}{2}\tan^{-1}\frac{I}{R}\right) + i\,\cos\left(\frac{1}{2}\tan^{-1}\frac{I}{R}\right)\right] & \text{for } R < 0, \end{cases} \tag{23c}$$

$$R = (k^2 - \nu_m\nu_T) - \beta^2(k^2+\nu_m^2)(k^2+\nu_T^2), \tag{23d}$$

$$I = (\nu_m + \nu_T)k. \tag{23e}$$

In the viscous system, the propagating mode and evanescent mode cannot be explicitly separated because the vertically propagating component with the vertical wavenumber M_R and the vertically decaying component with a decay rate M_I exist simultaneously in the entire range of k. In this study, we consider the case in which the coefficient of Rayleigh friction is equal to that of Newtonian cooling. Hereafter, we refer to $\nu = \nu_m = \nu_T$ as the viscous coefficient.

Figure 3 shows M_R, M_I, and R as a function of the horizontal wavenumber k in the cases of $\nu = 0.01$, 0.3, 0.7, and 0.9. The nonhydrostaticity factor β is specified as 0.5. For $\nu = 0.01$, M_R and M_I are similar to m and m' in the inviscid-limit case, respectively [Fig. 3(a)]. Similar to the inviscid-limit case, M_R (M_I) is dominant in the range of $k \le k_c$ ($k > k_c$), whereas M_I (M_R) is almost zero in the range of $k \ge k_c$ ($k < k_c$) [Fig. 3(a)]. Noting that the vertical wavenumber M_R is larger (smaller) than M_I when R is positive (negative), we classify the propagating mode and evanescent mode based on the sign of R. The k-range in which R is positive is referred to as the propagating mode in the viscous system. The evanescent mode with k being smaller (larger) than the k-minimum (maximum) in the k-range of the propagating mode is referred to as evanescent mode 1 (2). As ν increases, the k-range of the propagating

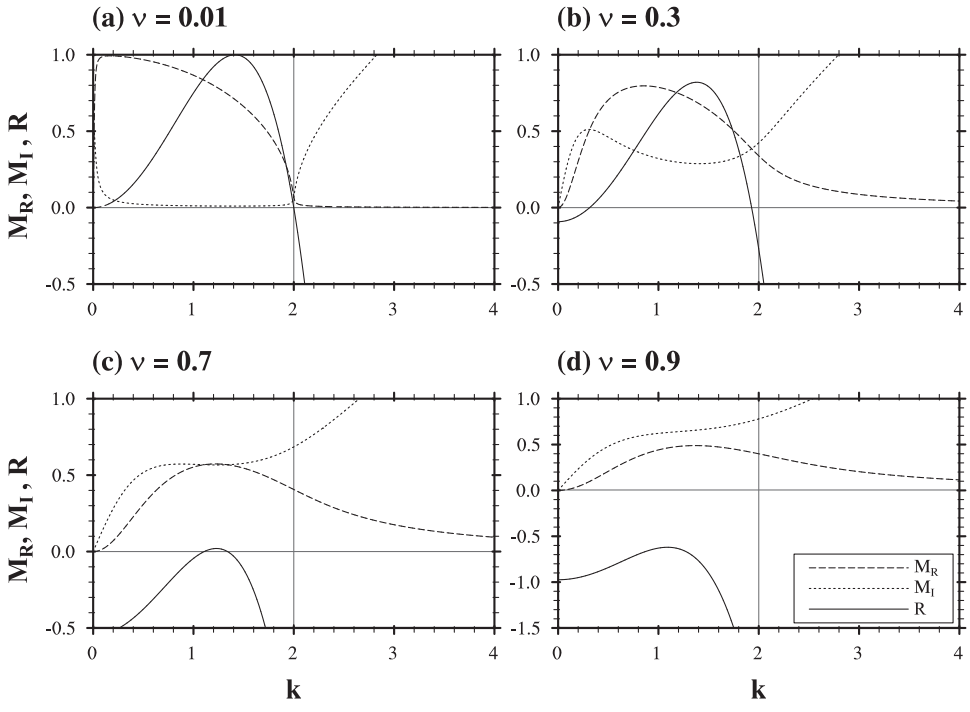

FIG. 3. M_R, M_I, and R as a function of the horizontal wavenumber k in the cases of $\beta = 0.5$ and ν = (a) 0.01, (b) 0.3, (c) 0.7, and (d) 0.9.

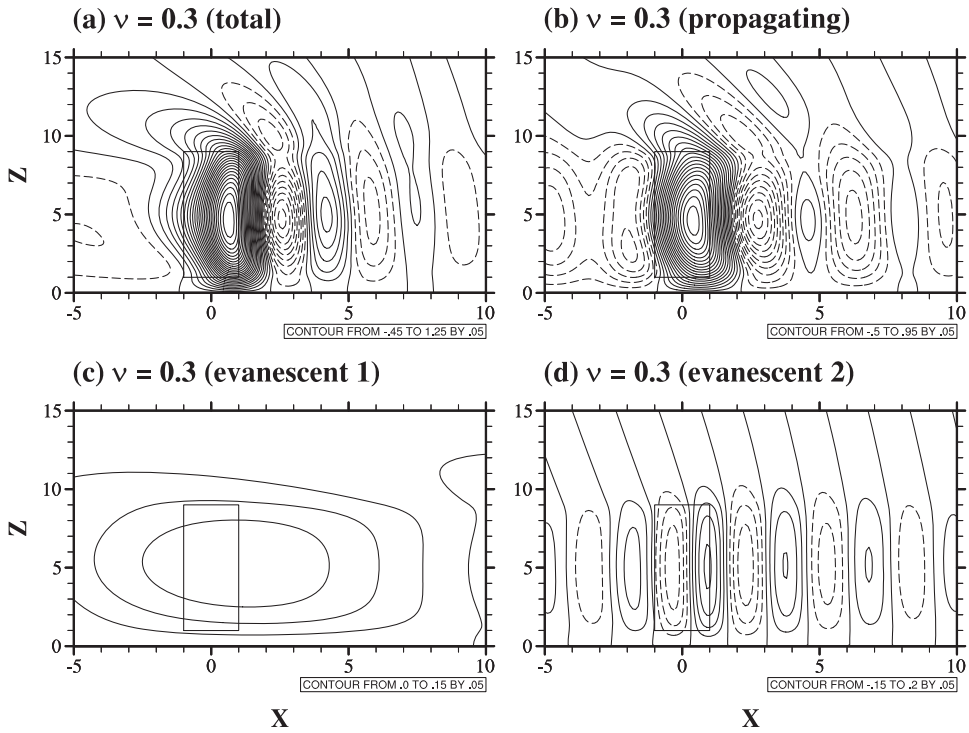

FIG. 4. Vertical velocity fields in the case of $\beta = 0.5$ and $\nu = 0.3$: (a) total, (b) propagating mode, (c) evanescent mode 1, and (d) evanescent mode 2. The rectangle in each panel represents the concentrated convective forcing region. The contour line information is given at the bottom of each panel.

mode becomes narrow and only the evanescent mode exists if ν exceeds a critical value. The critical viscous coefficient $\nu_c = 1/(2\sqrt{2}\beta)$ can be obtained under the condition that $R = 0$ does not have a solution. For $\beta = 0.5$, ν_c is 0.707.

Figure 4 shows the total vertical velocity field and the vertical velocity fields of the propagating mode, evanescent mode 1, and evanescent mode 2 in the case of $\beta = 0.5$ and $\nu = 0.3$. Similar to the inviscid-limit case, the alternating updrafts and downdrafts are clearly observed [Fig. 4(a)]. The boundary of k between the propagating mode and evanescent mode 1 (2) is $k = 0.31$ (1.93) and the corresponding horizontal wavelength is 20.27 (3.26). In this case, the contribution of evanescent mode 1 to the total flow is not significant, while the other two modes, that is, the propagating mode and evanescent mode 2, play roles similar to the two modes in the inviscid-limit system. The alternating updrafts and downdrafts have a horizontal wavelength longer than that in the inviscid-limit system, and they weaken further downstream.

Figure 5 is the same as Fig. 4 except for $\nu = 0.7$, a larger viscous coefficient. Strong updraft near the convective forcing

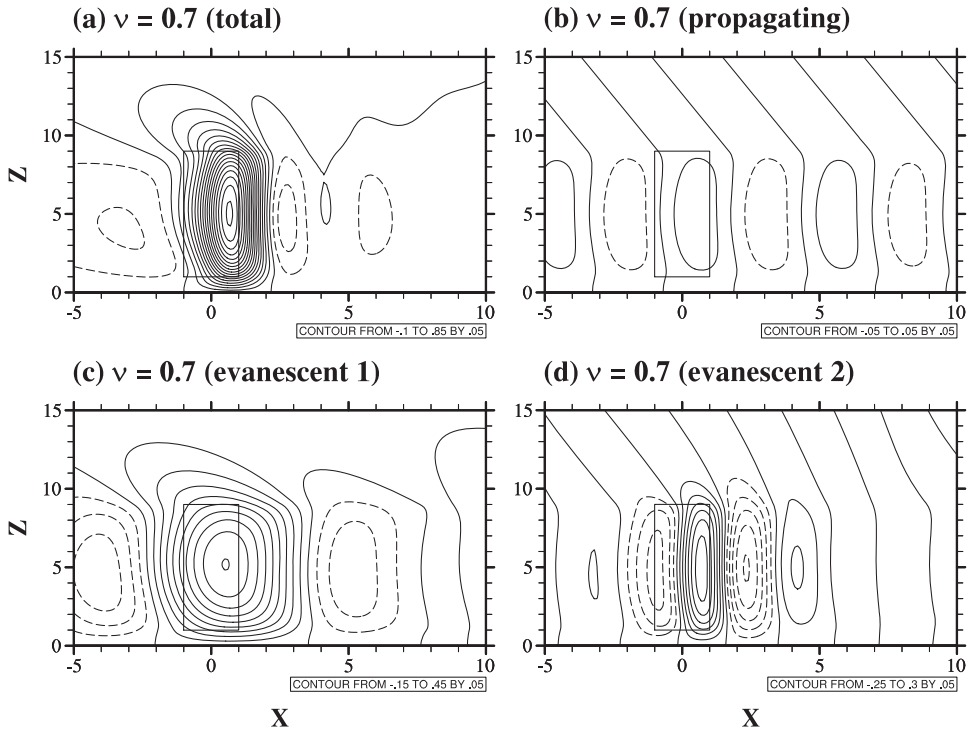

FIG. 5. The same as Fig. 4 except for $\nu = 0.7$.

center, broad compensating downdraft upstream of the convective forcing, and narrow compensating downdraft downstream of the convective forcing are the major characteristics of the total vertical velocity field [Fig. 5(a)]. The boundary of k between the propagating mode and evanescent mode 1 (2) is $k = 1.11$ (1.34) and the corresponding horizontal wavelength is 5.66 (4.69). When the flow system is strongly viscous, the alternating updrafts and downdrafts are almost dissipated due to the very narrow k-range of the propagating mode. Evanescent modes 1 and 2 are dominant modes, and the contribution of the propagating mode to the total field is minor.

C. Gravity-wave momentum flux

To examine nonhydrostatic effects on the gravity-wave momentum flux, the vertical flux of integrated horizontal momentum is derived by integrating the product of the spectral vertical velocity and the spectral horizontal velocity obtained using the Fourier-transformed continuity equation [$\hat{u}_j = (i/k)\partial\hat{w}_j/\partial z$]

$$M_j = \int_0^\infty M_{jk}dk = \int_0^\infty \lim_{L_x\to\infty}\frac{1}{L_x}\int_{-L_x/2}^{L_x/2} u_j w_j dx dk = \frac{1}{2}\int_0^\infty u_{jk}w_{jk}dk, \tag{24}$$

where L_x is the sufficiently large horizontal domain size and $j = 1, 2, 3$ depending on z [Eq. (18)]. Here, the orthogonality of the sinusoidal function is used.

In the inviscid-limit system, the gravity-wave momentum flux M_{2k} of the propagating mode for $h_1 < z \le h_2$ is

$$M_{2k} = -\frac{a^2}{2m^3k}e^{-2ak}(\cos mh_2 - \cos mh_1)(\cos mz - \cos mh_1). \tag{25}$$

The gravity-wave momentum flux below the convective forcing is $M_{1k} = M_{2k}\ (z = h_1) = 0$. The gravity-wave momentum flux above the convective forcing is $M_{3k} = M_{2k}\ (z = h_2) =$ constant and satisfies the Eliassen-Palm theorem.[12] Note that the evanescent mode does not contribute to the momentum flux.

Figures 6(a) and 6(b) show the vertical profiles of the gravity-wave momentum flux and its differences between the nonhydrostatic and hydrostatic-limit systems for various values of β. The inviscid-limit system is considered. As β increases, the gravity-wave momentum flux departs from that in the hydrostatic-limit system [Fig. 6(a)], so the magnitude of the gravity-wave momentum flux above $z \sim 3$ increases compared to that in the hydrostatic-limit system [Fig. 6(b)]. This means that in a nonhydrostatic system of large β, nonhydrostatically forced waves provide an additional momentum flux, although the additional momentum flux is small compared to the total momentum flux. Figure 6(c) shows the spectral gravity-wave momentum flux above the convective forcing M_{3k} as a function of k in the case of $\beta = 0.5$. The magnitude of the spectral gravity-wave momentum flux M_{3k} decreases with increasing k up to $k \sim 1.6$ and a secondary local maximum exists near $k = k_c$. We can calculate k at the secondary local maximum using $dM_{3k}/dk = 0$. In the case of $\beta = 0.5$, the wave component corresponding to the secondary local maximum is a slantwise (almost horizontally) propagating wave of $k = 1.958$ and $m = 0.204$. The slope of the wave propagation is $m/k = 0.104$. Because m is very small and positive when $k \sim k_c$, we can approximate M_{2k} for a very small $m = \varepsilon > 0$ using Eq. (25)

$$M_{2k} = -\frac{\varepsilon\beta a^2}{8}e^{-2ak}\left(h_2^2 - h_1^2\right)\left(z^2 - h_1^2\right). \tag{26}$$

The above approximation indicates that the nonhydrostatically generated additional gravity-wave momentum flux is

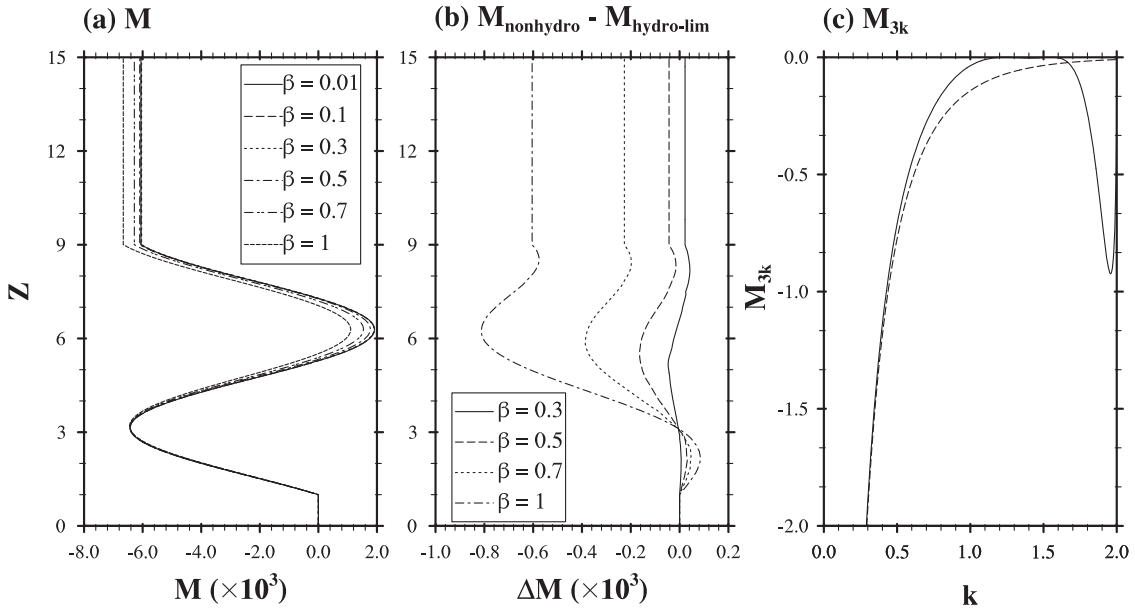

FIG. 6. (a) Vertical profiles of gravity-wave momentum flux in the cases of $\beta = 0.01$, 0.1, 0.3, 0.5, 0.7, and 1. (b) Differences in the gravity-wave momentum flux between the nonhydrostatic system in each case of $\beta = 0.3$, 0.5, 0.7, and 1 and the hydrostatic-limit system. (c) Spectral gravity-wave momentum flux above the convective forcing as a function of the horizontal wavenumber k in the case of $\beta = 0.01$ (dashed) and $\beta = 0.5$ (solid). The inviscid-limit system is considered.

proportional to the nonhydrostaticity factor. The above approximation also indicates that the magnitude of the nonhydrostatically forced momentum flux increases with increasing height and that above the convective forcing, it is larger for deeper convective forcing.

The nonhydrostatic effects on gravity-wave momentum fluxes are revealed in Fig. 6. The spectral gravity-wave momentum flux in a hydrostatic system can be obtained by applying $\beta = 0$ ($m = 1$) to Eq. (25). For small β ($\beta = 0.3$), the magnitude of the gravity-wave momentum flux in the nonhydrostatic system is slightly smaller than that in the hydrostatic (-limit) system [Fig. 6(b)]. For large enough β, however, the secondary maximum near $k = k_c$ in the spectral gravity-wave momentum flux appears while the magnitude of the spectral gravity-wave momentum flux in the nonhydrostatic system is still smaller than that in the hydrostatic system in the range of k smaller than ~1.7 [Fig. 6(c)]. If we integrate $M_{3k,\text{nonhydro}} - M_{3k,\text{hydro}}$ in the range of $k = (0, \sim 1.7]$ and $[\sim 1.7, 2]$ with respect to k, 0.10 and −0.13 are obtained, respectively. As a result, the magnitude of the gravity-wave momentum flux in the nonhydrostatic system is larger than that in the hydrostatic system.

Figures 2(c) and 2(d) show that the alternating updrafts and downdrafts are upstream tilted above the convective forcing, so the tilted waves transport wave energy vertically. As already mentioned, these tilted alternating updrafts and downdrafts mainly provide an additional momentum flux above the height of the convective forcing top ($z = h_2$). Note that other upstream tilted waves exist just above the convective forcing and that the sign of the vertical velocity above the convective forcing is opposite to the total vertical velocity [compare Figs. 1(c) and 2(c) and Figs. 1(d) and 2(d)]. For this reason, the additional spectral momentum flux in the low k-range is small even though the nonhydrostatically generated alternating updrafts and downdrafts provide a meaningful amount of momentum flux.

The result of our study shows that convective forcing in a non-hydrostatic system can provide an additional gravity-wave momentum flux above the convective forcing. Considering the importance of subgrid-scale convectively forced gravity-wave drag in large-scale or climate models, our result can be helpful in improving or developing a convectively forced gravity-wave drag parameterization in a nonhydrostatic framework.

In the viscous system, using Eq. (24), we can obtain the gravity-wave momentum flux

$$\begin{aligned} M_{1k} = \frac{a^2}{4k} e^{-2ak}(X_R^2 + X_I^2)(M_R \sinh 2M_I z \\ - M_I \sin 2M_R z)\left\{e^{-2M_I h_1} + e^{-2M_I h_2} \right. \\ \left. - 2e^{-M_I(h_1+h_2)} \cos M_R(h_2 - h_1)\right\} \quad \text{for } 0 \le z \le h_1, \end{aligned} \tag{27a}$$

$$\begin{aligned} M_{2k} = -\frac{a^2}{4k} e^{-2ak}(X_R^2 + X_I^2)\Big\langle M_R\Big[e^{-2M_I z}\Big\{\cosh 2M_I h_1 - e^{-M_I(h_1+h_2)} \cos M_R(h_2 - h_1) + \cos 2M_R h_1 - e^{-M_I(h_2-h_1)} \cos M_R(h_1 + h_2)\Big\} \\ - e^{-2M_I h_2} \sinh 2M_I z + \Big\{e^{-M_I(z+h_2)} \cos M_R(z + h_2) - e^{-M_I(z+h_1)} \cos M_R(z + h_1) + e^{M_I(z-h_2)} \cos M_R(z - h_2) \\ - e^{-M_I(z-h_1)} \cos M_R(z - h_1)\Big\}\Big] - M_I\Big[e^{-M_I(h_1+h_2)} \sin M_R\{2z - (h_2 - h_1)\} + e^{-M_I(h_2-h_1)} \sin M_R\{2z - (h_1 + h_2)\} \\ - e^{-2M_I h_2} \sin 2M_R z + \Big\{e^{-M_I(z+h_2)} \sin M_R(z + h_2) - e^{-M_I(z+h_1)} \sin M_R(z + h_1) \\ - e^{M_I(z-h_2)} \sin M_R(z - h_2) - e^{-M_I(z-h_1)} \sin M_R(z - h_1)\Big\}\Big]\Big\rangle \quad \text{for } h_1 < z \le h_2, \end{aligned} \tag{27b}$$

$$\begin{aligned} M_{3k} = -\frac{a^2}{4k} e^{-2ak}(X_R^2 + X_I^2) M_R e^{-2M_I z}\{\cosh 2M_I h_1 \\ + \cos 2M_R h_1 + \cosh 2M_I h_2 + \cos 2M_R h_2 \\ - 2 \cos M_R(h_1 + h_2) \cosh M_I(h_2 - h_1) \\ - 2 \cos M_R(h_2 - h_1) \cosh M_I(h_1 + h_2)\} \quad \text{for } z > h_2. \end{aligned} \tag{27c}$$

Figure 7 shows the vertical profiles of the gravity-wave momentum flux in the cases of $\nu = 0.01, 0.3$, and 0.7 for various values of β. For $\nu = 0.01$, the magnitude of the gravity-wave momentum flux above the convective forcing increases with increasing β, which is similar to that in the inviscid-limit system. This is due to the nonhydrostatically forced slantwise propagating gravity waves of $k \lesssim k_c$ which contribute to the secondary local maximum of the spectral momentum flux [Fig. 7(a)]. For larger ν, however, the magnitude of the gravity-wave momentum flux above the convective forcing decreases as β increases [Figs. 7(b) and 7(c)].

Figure 8 shows the vertical profiles of the gravity-wave momentum flux of the total and each mode in the cases of $\beta = 0.5$ and $\nu = 0.01$, 0.3, and 0.7. For $\nu = 0.01$, the propagating mode takes the largest portion of the total momentum flux [Fig. 8(a)]. As the viscous coefficient increases, the portion of the momentum flux of evanescent mode 1 increases [Figs. 8(b) and 8(c)]. For $\nu = 0.7$, the gravity-wave momentum flux of the propagating mode is almost dissipated, whereas the gravity-wave momentum flux of evanescent mode 1 is dominant. The critical viscous coefficient $\nu_c = 1/(2\sqrt{2}\beta)$ for $\beta = 0.1, 0.3, 0.5, 0.7$, and 1 are 3.54, 1.18, 0.71, 0.51, and 0.35, respectively. Therefore, the propagating mode is effectively dissipated by relatively weak viscous effects. Accordingly, the nonhydrostatic effects on convectively forced flows are easily weakened in a nonhydrostatic system of large β.

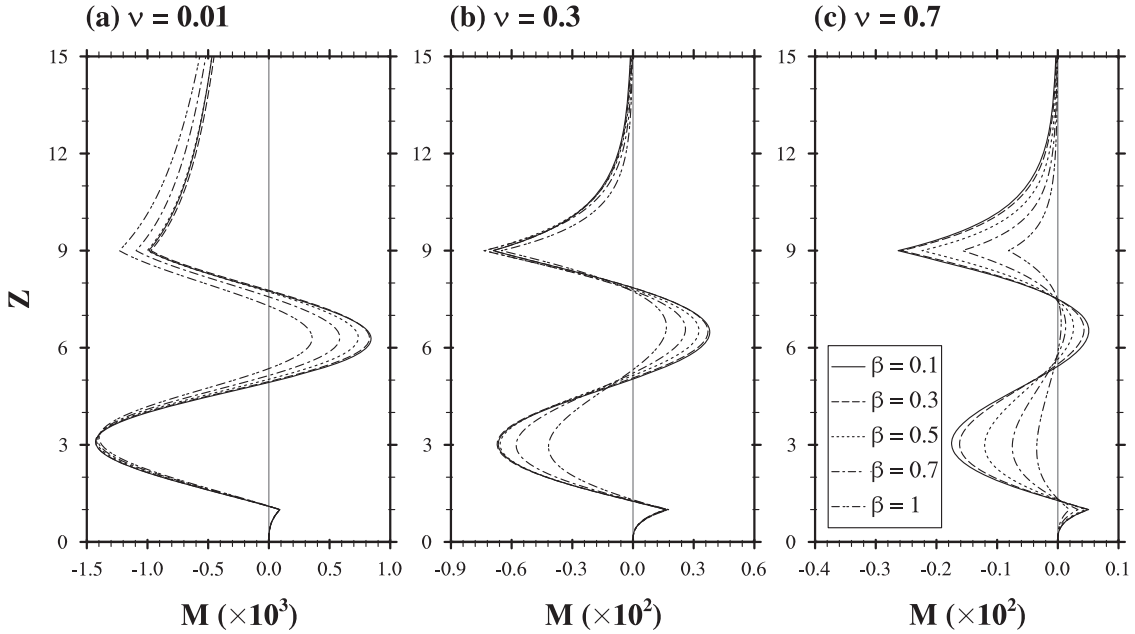

FIG. 7. Vertical profiles of gravity-wave momentum flux in the cases of ν = (a) 0.01, (b) 0.3, and (c) 0.7 for β = 0.1, 0.3, 0.5, 0.7, and 1.

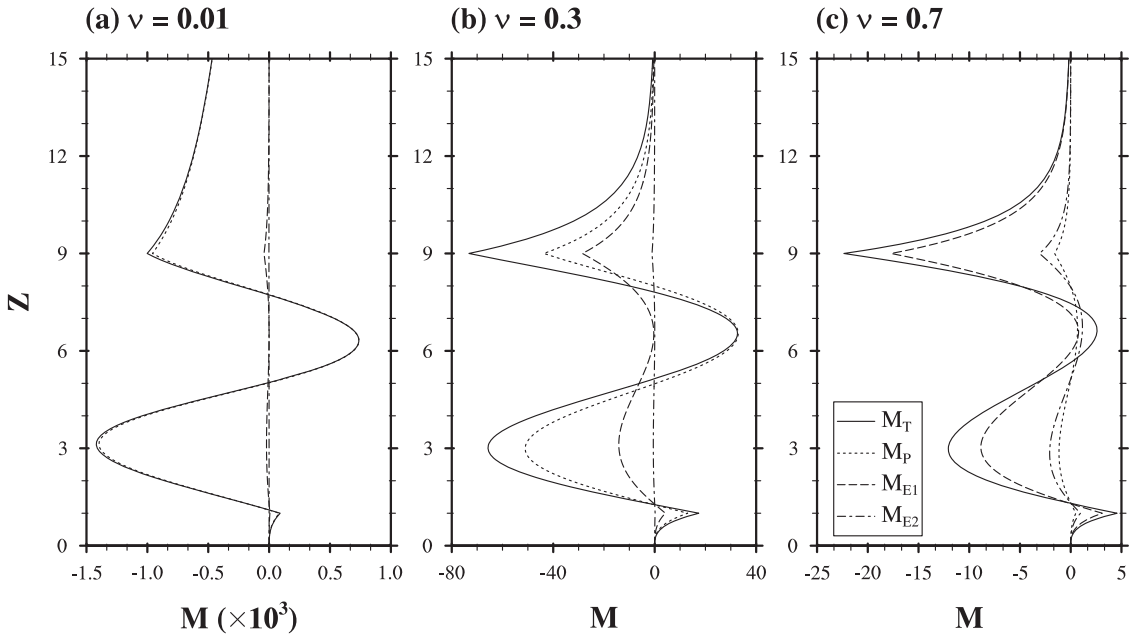

FIG. 8. Vertical profiles of the gravity-wave momentum flux of total and each mode in the cases of β = 0.5 and ν = (a) 0.01, (b) 0.3, and (c) 0.7.

IV. SUMMARY AND CONCLUSIONS

We examined nonhydrostatic effects on convectively forced mesoscale flows and the gravity-wave momentum flux by solving the equations governing small-amplitude perturbations in a linearized, two-dimensional, steady-state, nonrotating, Boussinesq airflow system with prescribed convective forcing. The nonhydrostaticity factor $\beta = U/Na$ appears in the nondimensionalized vertical momentum equation.

In an inviscid-limit system, the solution is divided into the propagating mode for $k \le k_c$ and the evanescent mode for $k > k_c$, where $k_c = \beta^{-1}$ is the nondimensional critical horizontal wavenumber. For very small β, the flow is close to the hydrostatic flow. As β increases, an alternating wavy pattern of updrafts and downdrafts appears downstream of the convective forcing and its nondimensional horizontal wavelength is $2\pi\beta$. The alternating updrafts and downdrafts correspond to almost horizontally propagating gravity waves of the propagating mode with the nondimensional horizontal wavenumber $k \sim k_c$. The momentum flux analysis indicates that the slantwise (almost horizontally) propagating gravity waves provide an additional momentum flux above the convective forcing and that its magnitude increases with increasing β and increasing convective-forcing depth.

In a viscous system, unlike in the inviscid-limit system, the solution cannot be explicitly separated into two modes.

Each wave component has a vertically propagating part and a vertically decaying part simultaneously. In this study, the propagating mode and two evanescent modes are classified by comparing the nondimensional vertical wavenumber M_R and the decay rate M_I. The k-range of the propagating mode becomes narrow as the viscous coefficient increases. As a result, the alternating updrafts and downdrafts downstream of the convective forcing are dissipated due to the viscous effect. For $\nu \geq \nu_c$, where $\nu_c = 1/(2\sqrt{2}\beta)$, the propagating mode disappears. For large ν, the magnitude of the momentum flux above the convective forcing decreases as β increases because the momentum flux of the propagating mode is easily dissipated in the case of larger β.

In this study, we investigated the nonhydrostatically enhanced gravity-wave momentum flux in an atmosphere with constant basic-state wind speed and static stability. With various environmental conditions and also various convective forcing geometries, the nonhydrostaticity can differently affect the convective gravity-wave momentum flux. In many convective gravity-wave drag parameterizations, the nonhydrostatic effects have not been well reflected so far. A challenging problem is to include the nonhydrostaticity β in a convective gravity-wave drag parameterization.

The characteristics of gravity waves forced by convective forcing are related to many factors which include the spatial extent and temporal time scale of the convective forcing.[39] This study considers only two dimensions. In three dimensions, gravity waves forced by three-dimensional convective forcing are dispersed in three-dimensional space. Therefore, the characteristics of gravity waves forced by three-dimensional convective forcing in three dimensions can differ from those forced by two-dimensional convective forcing in two dimensions. Further studies taking account of time-dependent convective forcing in a nonsteady, three-dimensional dynamical framework would be helpful in better understanding convectively forced flows or gravity waves in a nonhydrostatic framework.

In this study, we considered an airflow system with uniform basic-state wind speed and static stability. To study the general characteristics of nonhydrostatic effects on convectively forced flows in a more realistic framework, the vertical variations of basic-state wind speed and static stability need to be included. In their study of mountain waves, Wurtele *et al.*[15] and Keller[14] showed that there are a number of nonhydrostatically forced resonant waves with various horizontal wavelengths in a nonhydrostatic atmosphere with basic-state wind shear and a stability jump at the tropopause. Unlike mountain forcing, which is mechanical forcing at the surface, convective forcing is thermal forcing that can generate gravity waves in a range of altitudes where the forcing is located. Thus, convectively forced flows in a nonhydrostatic non-uniform atmosphere can reveal some different features from topographically forced flows, and this topic deserves an investigation.

ACKNOWLEDGMENTS

The authors are grateful to two anonymous reviewers for providing valuable comments on this study. This work was funded by the Korea Meteorological Administration Research and Development Program under Grant No. KMIPA 2015-5100 and by the Small Grant for Exploratory Research (SGER) program through the National Research Foundation of Korea (NRF) funded by the Ministry of Science and ICT (MSIT) (No. 2018R1D1A1A02086007).

[1] D. A. Aguilar and B. R. Sutherland, "Internal wave generation from rough topography," Phys. Fluids **18**, 066603 (2006).
[2] H. Knight, D. Broutman, and S. D. Eckermann, "Generalized stationary phase approximations for mountain waves," Phys. Fluids **28**, 046601 (2016).
[3] Z. Chen, J. Xie, J. Xu, Y. He, and S. Cai, "Selection of internal wave beam directions by a geometric constraint provided by topography," Phys. Fluids **29**, 066602 (2017).
[4] Y. Dossmann, F. Pollet, P. Odier, and T. Dauxois, "Mixing and formation of layers by internal wave forcing," J. Geophys. Res.: Oceans **122**, 9906–9917, https://doi.org/10.1002/2017jc013309 (2017).
[5] S. Harnanan, M. Stastna, and N. Soontiens, "The effects of near-bottom stratification on internal wave induced instabilities in the boundary layer," Phys. Fluids **29**, 016602 (2017).
[6] Y.-L. Lin, *Mesoscale Dynamics* (Cambridge University Press, 2007), p. 630.
[7] Y.-L. Lin and R. B. Smith, "Transient dynamics of airflow near a local heat source," J. Atmos. Sci. **43**, 40–49 (1986).
[8] J.-Y. Han and J.-J. Baik, "Theoretical studies of convectively forced mesoscale flows in three dimensions. Part II: Shear flow with a critical level," J. Atmos. Sci. **67**, 694–712 (2010).
[9] P. Queney, "The problem of air flow over mountains: A summary of theoretical studies," Bull. Am. Meteorol. Soc. **29**, 16–26 (1948).
[10] R. B. Smith, "The influence of mountains on the atmosphere," Adv. Geophys. **21**, 87–230 (1979).
[11] I. Stiperski, S. Serafin, A. Paci, H. Ágústsson, A. Belleudy, R. Calmer, K. Horvath, C. Knigge, J. Sachsperger, L. Strauss, and V. Grubišić, "Water tank experiments on stratified flow over double mountain-shaped obstacles at high-Reynolds number," Atmosphere **8**, 13 (2017).
[12] A. Eliassen and E. Palm, "On the transfer of energy in stationary mountain waves," Geofys. Publ. **22**, 1–23 (1961).
[13] J. B. Klemp and D. R. Lilly, "The dynamics of wave-induced downslope winds," J. Atmos. Sci. **32**, 320–339 (1975).
[14] T. L. Keller, "Implications of the hydrostatic assumption on atmospheric gravity waves," J. Atmos. Sci. **51**, 1915–1929 (1994).
[15] M. G. Wurtele, R. D. Sharman, and T. L. Keller, "Analysis and simulations of a troposphere-stratosphere gravity wave model. Part I," J. Atmos. Sci. **44**, 3269–3281 (1987).
[16] D. Broutman, J. W. Rottman, and S. D. Eckermann, "Maslov's method for stationary hydrostatic mountain waves," Q. J. R. Meteorol. Soc. **128**, 1159–1171 (2002).
[17] D. Broutman, J. W. Rottman, and S. D. Eckermann, "A simplified Fourier method for nonhydrostatic mountain waves," J. Atmos. Sci. **60**, 2686–2696 (2003).
[18] S. B. Vosper, "Inversion effects on mountain lee waves," Q. J. R. Meteorol. Soc. **130**, 1723–1748 (2004).
[19] M. C. Teixeira, A. Paci, and A. Belleudy, "Drag produced by waves trapped at a density interface in non-hydrostatic flow over an axisymmetric hill," J. Atmos. Sci. **74**, 1839–1857 (2017).
[20] M. J. Alexander, J. H. Richter, and B. R. Sutherland, "Generation and trapping of gravity waves from convection with comparison to parameterization," J. Atmos. Sci. **63**, 2963–2977 (2006).
[21] A. W. Grimsdell, M. J. Alexander, P. T. May, and L. Hoffmann, "Model study of waves generated by convection with direct validation via satellite," J. Atmos. Sci. **67**, 1617–1631 (2010).
[22] M. J. Alexander and J. R. Holton, "On the spectrum of vertically propagating gravity waves generated by a transient heat source," Atmos. Chem. Phys. **4**, 923–932 (2004).
[23] D. C. Fritts and M. J. Alexander, "Gravity wave dynamics and effects in the middle atmosphere," Rev. Geophys. **41**, 1003, https://doi.org/10.1029/2001rg000106 (2003).
[24] J. H. Beres, "Gravity wave generation by a three-dimensional thermal forcing," J. Atmos. Sci. **61**, 1805–1815 (2004).

[25]H.-Y. Chun and J.-J. Baik, "Momentum flux by thermally induced internal gravity waves and its approximation for large-scale models," J. Atmos. Sci. **55**, 3299–3310 (1998).
[26]H.-Y. Chun and J.-J. Baik, "An updated parameterization of convectively forced gravity wave drag for use in large-scale models," J. Atmos. Sci. **59**, 1006–1017 (2002).
[27]I.-S. Song and H.-Y. Chun, "Momentum flux spectrum of convectively forced internal gravity waves and its application to gravity wave drag parameterization. Part I: Theory," J. Atmos. Sci. **62**, 107–124 (2005).
[28]I.-S. Song and H.-Y. Chun, "A Lagrangian spectral parameterization of gravity wave drag induced by cumulus convection," J. Atmos. Sci. **65**, 1204–1224 (2008).
[29]H.-J. Choi and H.-Y. Chun, "Momentum flux spectrum of convective gravity waves. Part I: An update of a parameterization using mesoscale simulations," J. Atmos. Sci. **68**, 739–759 (2011).
[30]M.-J. Kang, H.-Y. Chun, and Y.-H. Kim, "Momentum flux of convective gravity waves derived from an off-line gravity wave parameterization. Part I: Spatiotemporal variations at source level," J. Atmos. Sci. **74**, 3167–3189 (2017).
[31]S. Woo, J.-J. Baik, H. Lee, J.-Y. Han, and J. M. Seo, "Nonhydrostatic effects on convectively forced mesoscale flows," J. Korean Meteor. Soc. **23**, 293–305 (2013) (In Korean with English abstract.).
[32]I.-S. Song, H.-Y. Chun, and T. P. Lane, "Generation mechanisms of convectively forced internal gravity waves and their propagation to the stratosphere," J. Atmos. Sci. **60**, 1960–1980 (2003).
[33]J.-Y. Han and J.-J. Baik, "Theoretical studies of convectively forced mesoscale flows in three dimensions. Part I: Uniform basic-state flow," J. Atmos. Sci. **66**, 947–965 (2009).
[34]J.-J. Baik, H.-S. Hwang, and H.-Y. Chun, "Transient, linear dynamics of a stably stratified shear flow with thermal forcing and a critical level," J. Atmos. Sci. **56**, 483–499 (1999).
[35]J.-Y. Han and J.-J. Baik, "Nonlinear effects on convectively forced two-dimensional mesoscale flows," J. Atmos. Sci. **69**, 3391–3404 (2012).
[36]A. Babin, A. Mahalov, and B. Nicolaenko, "On the asymptotic regimes and the strongly stratified limit of rotating Boussinesq equations," Theor. Comput. Fluid Dyn. **9**, 223–251 (1997).
[37]H. Wells and S. B. Vosper, "The accuracy of linear theory for predicting mountain-wave drag: Implications for parameterization schemes," Q. J. R. Meteorol. Soc. **136**, 429–441 (2010).
[38]R. Laprise and W. R. Peltier, "On the structural characteristics of steady finite-amplitude mountain waves over bell-shaped topography," J. Atmos. Sci. **46**, 586–595 (1989).
[39]S. L. Vadas and D. C. Fritts, "Reconstruction of the gravity wave field from convective plumes via ray tracing," Ann. Geophys. **27**, 147–177 (2009).